Journal of Magnetism and Magnetic Materials 420 (2016) 158–165

Contents lists available at ScienceDirect

Journal of Magnetism and Magnetic Materials

journal homepage: www.elsevier.com/locate/jmmm

Observation of ice-rule violation and monopole dynamics via edge nucleation of domain walls in artificial spin ice lattice

S. Krishnia, I. Purnama, W.S. Lew*

School of Physical and Mathematical Sciences, Nanyang Technological University, 21 Nanyang Link, Singapore, 637371 Singapore

ARTICLE INFO

Article history:
Received 17 February 2016
Received in revised form
17 May 2016
Accepted 5 July 2016
Available online 6 July 2016

Keywords:
Domain walls
Spin ice
Magnetic monopoles

ABSTRACT

In a patterned Co honeycomb spin ice structure, we show that violation in the ice-rule or magnetic monopoles, can be observed during a magnetization reversal process in 430 Oe $\leq H \leq$ 760 Oe magnetic field (H) range. The monopoles are shown to originate from the nucleation of domain walls at the edges, and they hop towards the other edge via the propagation of magnetic domain walls. The paths that the domain walls traveled or the Dirac strings, are shown to increase in length with magnetic fields increment and no random flipping of the bars are observed in the structure.

1. Introduction

Emergent quasiparticles with similar properties as Dirac monopoles [1] have recently been observed in Pyrochlore frustrated magnetic materials such as $Dy_2Ti_2O_7$ [2–4]. In such materials, the quasiparticles, or the monopoles, are observed at the ends of a set of overturned dipoles, which propagated into opposite directions under external perturbations at low temperatures [2,4]. These observations have then inspired the investigations of finding isolated magnetic particles at room temperature. Detection and control of these magnetic charges might then lead to the realization of high-density memory and logic devices [5,6]. One approach to observe the monopole is by making use of patterned ferromagnetic nanoislands to represent the dipoles [7]. The nanoislands structures are also termed as artificial spin ice systems [8–12] because they share similar properties with frustrated magnetic compounds [2–4] as well as with water ice, such as the ice-rule and the degenerate ground energy states [13,14]. In the water ice, the ice-rule states that for every Oxygen (O) atom, there are two Hydrogen (H) atoms placed close to it and other two H atoms placed farther from it [15]. Each O–H bond can then be represented by an arrow that points either away or towards the O atom. Similarly, in artificial spin ice systems, the spins around each vertex are pointed either away or towards the vertex, as stated by the ice-rule [13,16]. The quasiparticles, *i.e.* the monopoles, are then formed when the ice-rule is broken via random spins flip in both connected [17] and disconnected [18] honeycomb/kagome spin ice structures [19,20]. These monopoles have been shown to propagate into the lattice under the influence of external magnetic field [17,18,21,22]. In the honeycomb spin ice structures, the random nucleation and motion of the monopoles were explained either by the variations in the interaction strengths at each vertex or by the variations in the coercivity of the individual bars [17,18,23]. These two variations arise due to the roughness and the small non-uniformity in the bar dimensions during the lithography process, which promotes the generation of magnetic monopoles at random positions [17,18]. In comparison, the direct observation of the controlled formation of magnetic monopoles still needs to be investigated.

In this work, we show that it is possible to control the formation of magnetic monopoles at room temperature in connected honeycomb artificial spin ice structure via magnetic domain wall (DW) propagation from the edge of the structure. The monopoles are trapped at the vertices of the artificial spin ice structure similar to frustrated magnetic compounds [2–4,14]. Under the application of external magnetic field, the monopoles are shown to propagate in the nanostructure via continuous propagation of the DWs. Magnetic force microscopy measurements are then employed to detect the monopoles and to image the path imprinted by the DWs during their propagation through the spin ice structures. With the support of micromagnetic simulations, clear evidence of the formations of isolated magnetic monopoles and Dirac strings are presented.

2. Experimental details

A thin film stack of Ta(5 nm)/Co(15 nm)/Ta(5 nm) is deposited using ultra high vacuum magnetron sputtering. The spin ice

* Corresponding author.
E-mail address: wensiang@ntu.edu.sg (W.S. Lew).

http://dx.doi.org/10.1016/j.jmmm.2016.07.005
0304-8853/

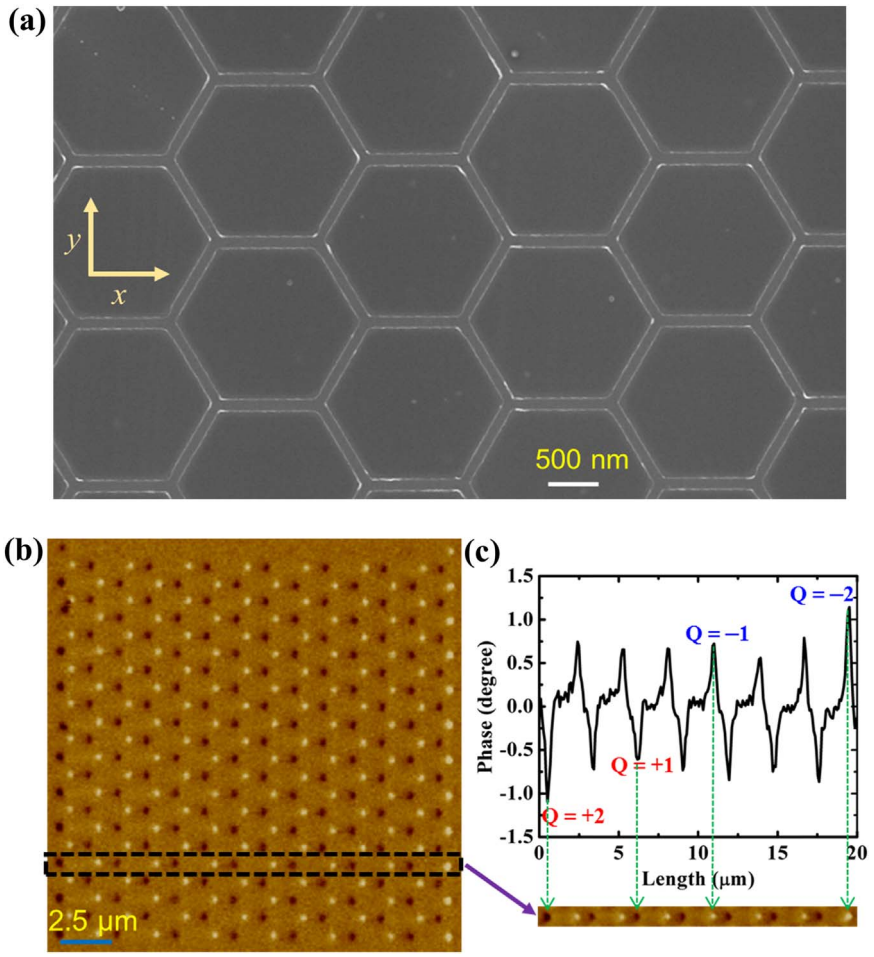

Fig. 1. (a) SEM image of connected Co honeycomb spin ice structure. (b) MFM image of artificial connected honeycomb spin ice structure saturated along negative *x*-direction with applied magnetic field of −2 kOe. The black and white contrasts at the vertices correspond to the attraction and repulsion between the MFM tip and the magnetic charges. (c) The phase shift reading of the MFM image within the enclosed area. The relative magnitude and sign of the corresponding magnetic charges are included respectively.

structure was fabricated on Si/SiO_2 (300 nm) substrates. The stack was coated with a negative resist prior to the patterning of the honeycomb spin ice structure by means of e-beam lithography. The pattern transfer was completed using Ar ion milling and wet chemical stripping techniques. The scanning electron microscopy (SEM) image of the patterned honeycomb spin ice structure is shown in Fig. 1(a). The length and width of each bar of the honeycomb structure are chosen as 1 μm and 100 nm respectively, to ensure the magnetization within each bar to form a single domain due to shape anisotropy. The spin ice array was initially saturated along $-x$ direction with a high magnetic field of $H_x = -2$ kOe. The magnetization direction of each bar is mapped using magnetic force microscopy (MFM) system at the remanence. The measurements were performed using an AppNano commercial tip with approximate magnetic moment of 10,313 emu, at lift-scan height of 140 nm to obtain an optimised magnetic topography signal. For our measurements the MFM tip was initially magnetized to have a south pole induced at its apex. In the honeycomb or kagome spin ice, three spins interact at each vertex and follow 2-in/1-out or 1-in/2-out pseudo ice-rule state [19]. The 2-in/1-out or 1-in/2-out state favor to carry a net magnetic charge at each vertex as shown in the Fig. 1(b). The vertex is said to have a net magnetic charge $Q = -1(+1)$ when the resultant magnetic flux was diverging *i.e.* 1-in/2-out state (converging *i.e.* 2-in/1-out state). More details of the charge convention are discussed in the Supplementary 1. The bright (magnetic charge, $Q = -1$) and dark ($Q = +1$) contrasts at the vertices in the Fig. 1(b), are correspond to the repulsive (south) and attractive (north) interactions between the MFM tip and the net magnetic charge at the vertices, respectively. The alternating order of contrasts at the honeycomb structure shows that each bar possesses a single domain at remanence. The MFM phase shift of the dotted area is plotted in Fig. 1(c). The magnitude and the sign of the magnetic charges of the corresponding area are also included in the figure, which can be inferred from the relative peak height of the MFM phase shift. The results show that the structure has $Q = -2$ at the right end and $Q = +2$ at the left end of the structures due to the edge effects and alternating $Q = \pm 1$ elsewhere.

3. Results and discussion

To create the magnetic excitations within the structure, the applied magnetic field is switched in the opposite direction *i.e.* along the $+x$ direction. The MFM images of the structure were captured during the stepwise reversal. Shown in Fig. 2(a), is the MFM image of the structure in quasi-remanent state after a magnetic field of $H_x = +430$ Oe was applied. The results show that disorders in the magnetic charge distribution are observed during the magnetization reversal process. The magnetic charge disorders can be seen as charges with similar contrasts being shown next to each other in the marked areas (dashed ellipses) of Fig. 2(a). Here,

the magnetic charge disorders appear only near the edges of the structure. Fig. 2(b) shows the enlarged image of one of the disorder regime (X): Fig. 2(b-i) shows the initial state of the area, while the right image (Fig. 2(b-ii)) shows the quasi-static disordered state of the same area after the field application of $+430$ Oe. The magnitude and sign of magnetic charges are also marked at each vertex in both the states. The blue and red color of arrows represent the direction of magnetization along the $-x$ axis and $+x$ axis, respectively. The result shows that a charge of $Q=+2$ (dark) has been transferred to a vertex above it and converts it from $Q=-1$ (bright) into $Q=+1$ (dark). Additionally, the result also shows that the total magnetic charges of the initial (Q_i) and final state (Q_f) is conserved *i.e.* $\{Q_i=(+2-1)\}=+1=\{Q_f=(0+1)\}$.

To understand the charge transfer mechanism, Mumax3 micromagnetic simulations [24] have been performed to visualize the intermediate states during magnetization reversal. The simulations were performed on ferromagnetic bars that were arranged in honeycomb geometry in a total area of 7.65 μm × 6.65 μm. The dimensions of each bar were set similar to the fabricated structure shown in the experimental results, with each having a length of 1 μm, a width of 100 nm and a thickness of 15 nm. The chosen simulation parameters for Co were: saturation magnetization, $M_s=1.4\times10^6$ A/m, exchange stiffness constant, $A=1.4\times10^{-11}$ J/m, and zero magnetocrystalline anisotropy [25]. The damping constant (α) was set to 0.01 and the cell size was 5 nm × 5 nm × 5 nm. The detailed mechanism of the charge transfer phenomenon is illustrated in Fig. 2(c). As shown by the intermediate magnetization states at both edges ($x=0$ μm and $x=7.65$ μm), the edges of the artificial spin ice structure are the favorable nucleation sites for the DW generation. In our structure transverse DWs are the stable configurations [6,20,26]. When the external magnetic field is applied, head-to-head DWs are nucleated at the left edges of the structure ($x=0$ μm) while tail-to-tail DWs are nucleated at the right edges ($x=7.65$ μm). The head-to-head DW ($Q=+2$) moves along the $+x$ direction and collide with the nearest $Q=-1$ vertex and transform it into $Q=+1$, as shown in the top half image of Fig. 2(c). Consequently, the direction of the magnetization in the

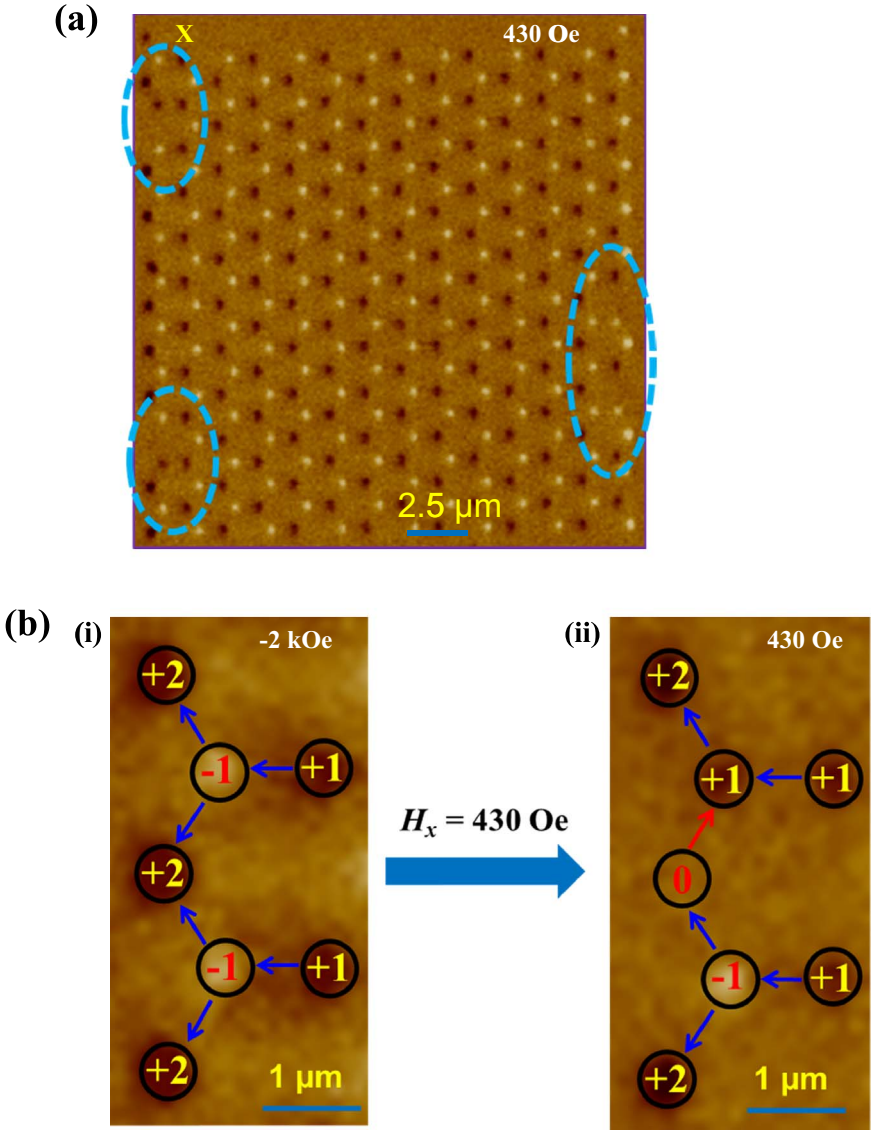

Fig. 2. (a) MFM image of uniformly magnetized artificial spin ice structure after magnetic field sweeping from negative saturation to a positive 430 Oe. (b) The enlarged images of area 'X' of the spin ice with the corresponding magnetic charges at negative saturation (i) and after the application of 430 Oe ex-situ field (ii). (c) The snapshots of micromagnetic simulations to show the intermediate states during the reversal process at both left and right edges of the structure.

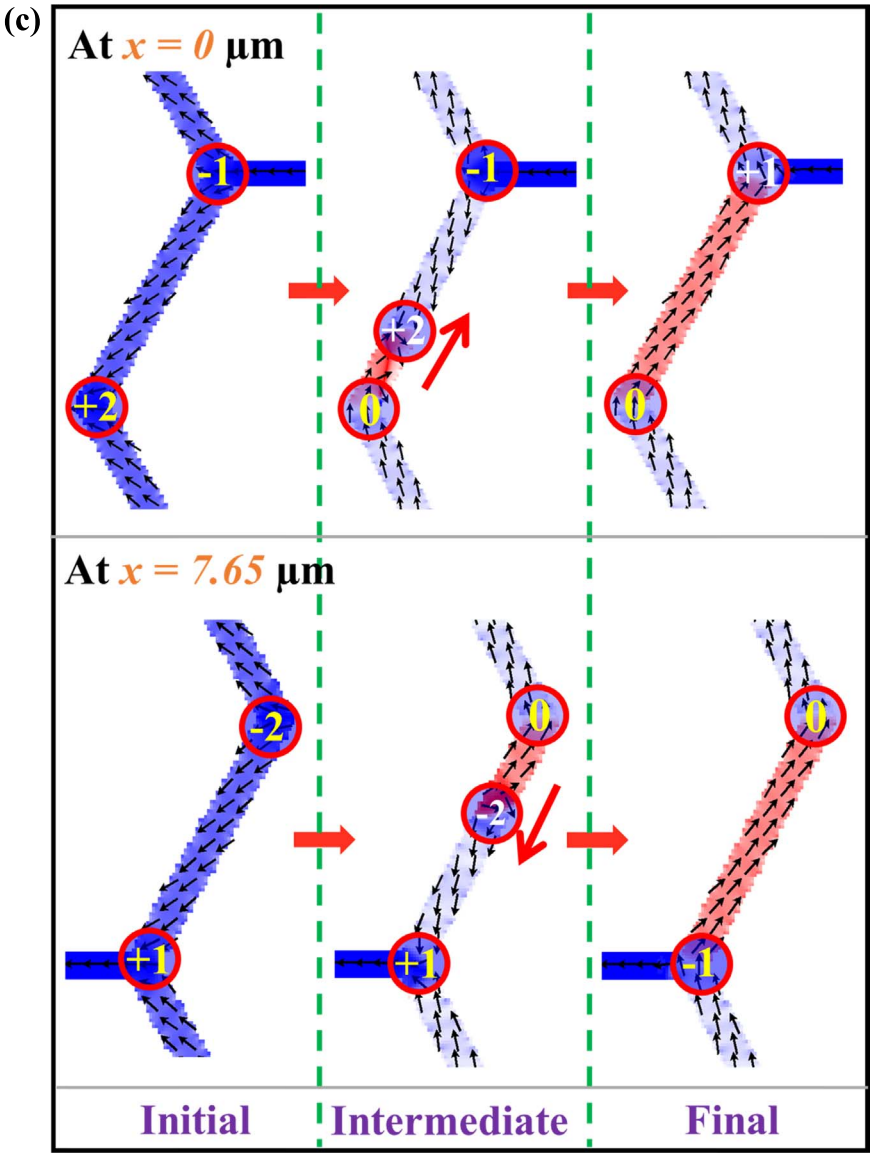

Fig. 2. (*continued*)

slanted bar is inverted by the propagation of the DW, as shown by the final state. Similarly, the tail-to-tail DWs ($Q=-2$), which are created at the right edge of the structure ($x=7.65$ μm), move in the $-x$ direction to change the $Q=+1$ vertex into $Q=-1$ (as shown in lower half of Fig. 2(c)). Here we assume that the magnetic charge of the head-to-head and tail-to-tail DWs are $Q=+2$ and of $Q=-2$, respectively. Detailed illustrations of the magnetization configuration between the initial and final states of different vertices and the magnetic charge model of the DW are presented in Supplementary 1.

The applied magnetic field is then increased in the steps of 5 Oe to create further excitations in the Co honeycomb lattice. At magnetic field of $H_x=530$ Oe, new particles are found to emerge in the honeycomb spin ice structure. As shown in Fig. 3(a), a big bright spot has appeared at point 'A' in the dotted area of the lattice. The MFM phase shift of the area around the point 'A' is also shown in Fig. 3(b). The result shows that the MFM phase shift of the point 'A' ($Q=-3$) is relatively three times higher than the others which implies that the magnetizations of all three bars at this vertex are pointing away from this point as labeled by the arrows. The charge $Q=-3$ can then be interpreted as a monopole as it gives non-vanishing magnetic charge density (ρ_m) over the range of lattice constant of the structure [3]. The charge $Q=-3$, *i.e.* the monopole, is unique as compared to the other magnetic charges within the structure by this virtue. The presence of the monopole hence violates the ice rule, and the energy that is required to pin the monopole at the corresponding vertex comes from the local lattice potential of surrounding vertices [27,28]. The presence of the monopole creates a high energy state and therefore it was not in the remanent state of the structure. However, it can be generated in our structure at 530 Oe due to the fact that the slanted and the horizontal bars are reversed at different magnetic fields (Supplementary 2 and 3). The dissimilar coercive fields of the slanted and horizontal bars create a potential for the DW and trap it at the vertex and hence violets the ice rule locally [27]. At magnetic field of 540 Oe, the magnetic monopole dissociated and moved to another vertex as shown in Fig. 3(c) (point B), and the path imprinted during the monopole migration is termed as 1D

Dirac strings [18,29].

Fig. 3(d) shows the different magnetization stages of the system during the formation and the propagation of the monopole. A DW ($Q=-2$) enters through one branch of the structure which inverts the magnetic charge of the vertex next to point 'A' from $Q=+1$ to $Q=-1$, as shown in Fig. 3(d-ii and d-iii). Further increment in the magnetic field allows the DW to be reemitted and moves to point 'A' as shown in Fig. 3(d-iv). A high energetic monopole is then formed at point 'A' as the magnetizations around that vertex now all point away from it (Fig. 3(d-v)). As mentioned previously, the presence of the monopole violates the ice-rule and creates a high energy state. Hence, less energy is required to dissociate the monopole to the surrounding bar [Supplementary 2]. Here, the monopole dissociates and a DW is emitted from point 'A' at an applied external field of 540 Oe, and invert the slanted bar (Fig. 3(d-vi))which is much less than of its critical field (1166 Oe) that is calculated by considering the dipole model [21,30,31] [Supplementary 3].

As the applied magnetic field is increased, new monopoles are generated within the system while existing 1D Dirac strings are extended. Fig. 4(a)–(d) shows the MFM images of the same region as in Fig. 3(a) and (c), in different quasi-remanent states. At external field of $H_x=580$ Oe, the Dirac string at the top (aqua arrows) was extended in the length, while a new Dirac string also appeared in the middle of the lattice (yellow arrows). Our MFM images show that the formation of the two Dirac strings here are mediated by the propagation of $Q=-2$ charge in the $-x$ direction (the end points of both the yellow and aqua strings are converted from dark to bright). The magnetization state of the system then remained unchanged for a range of 55 Oe. However, at applied magnetic field of $H_x = 635$ Oe, the monopoles were pushed by a large distance in avalanche-like behavior [18]. New strings (white and red) were also seen to emerge within the structure. Additionally, the red Dirac string also shows that it connects two oppositely charged monopoles: a positive (dark contrast) monopole is observed at the right end of the red string while a negative (bright contrast) monopole is observed at the left end. The positions of the two monopoles within the red Dirac string also show that the positive monopole move in the same direction as the applied field while the negative monopole move against it. Fig. 4

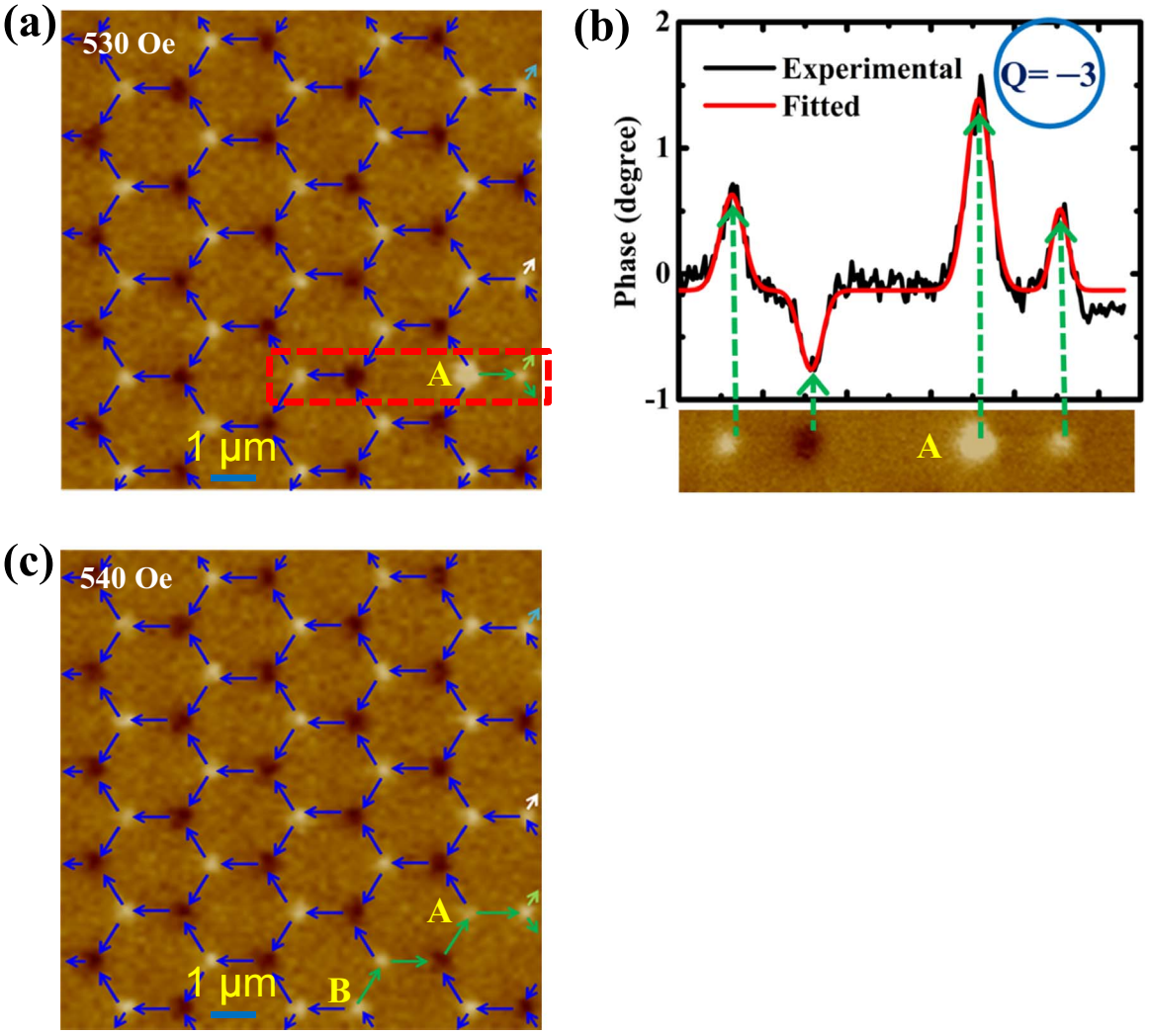

Fig. 3. (a) Formation of $Q=-3$ monopole-like defects, as shown by the big bright dot within the dotted area. The arrows represent the direction of magnetization in each bar. (b) Phase shift in the MFM image of the corresponding dotted area with a close look of the monopole along with the charge amplitude. (c) The dissociation of monopole-like defects via the formation of a Dirac string (green). (d) Micromagnetic simulations showing the violation of ice-rule and monopole formation in hexagonal spin ice via domain wall propagation (i) Initial state of the spin ice structure. (ii) Injection of a DW in one of the branch. (iii) Conversion of one of the vertex from $Q=+1$ *to* $Q=-1$. (iv) Emission of a DW in the horizontal bar from the right vertex. (v) Violation of ice-rule and formation of a $Q=-3$ charge at point 'A'. (vi) Dissociation of the monopole via emission of the DW. (For interpretation of the references to color in this figure legend, the reader is referred to the web version of this article.)

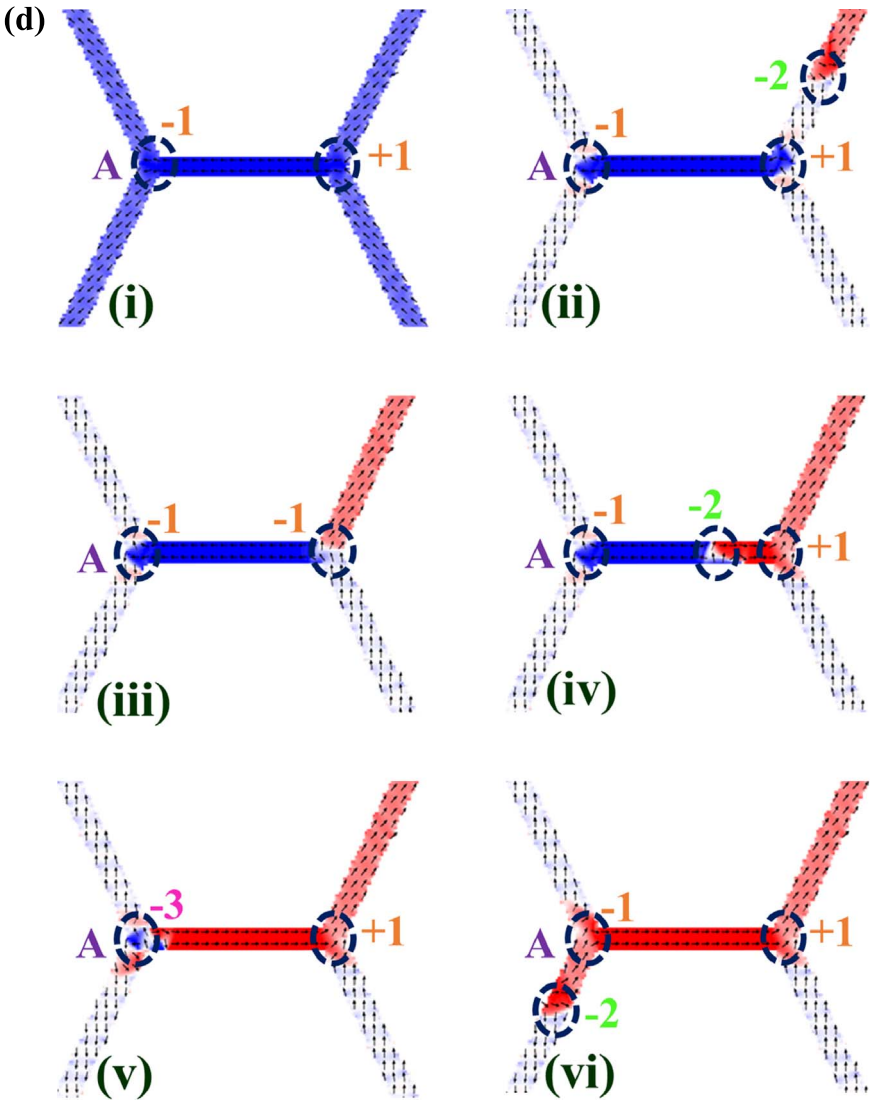

Fig. 3. (*continued*)

(c) shows that the formation of the white Dirac string is mediated through the propagation of a monopole with a magnetic charge of $Q=+2$ along the $+x$ direction, which can be inferred from the switching of point 'N' from bright contrast to dark contrast at a field $H_x=650$ Oe. The spin ice structure is saturated at 760 Oe along the $+x$ direction as shown in Fig. 4(d). The magnetization configuration of all the vertices was stable and unchanged when the magnetic fields higher than 760 Oe were applied to the structure. Fig. 4(e) shows the simulated hysteresis of the connected honeycomb artificial spin ice structure. The result shows steps-like behavior that corresponds to the avalanche nature of artificial spin ice structure [18]. Points 'a'–'d' in the hysteresis loop represent the possible magnetization states of the spin ice structure which are shown in Fig. 4(a)–(d).

4. Conclusion

In conclusion, we have shown that it is possible to break the ice-rule in connected honeycomb artificial spin ice structures. The monopoles which are created upon the violation of ice-rule can then be detected by the use of MFM. These monopoles are mobile in nature in the presence of external magnetic field, and the paths traveled by the monopoles *i.e.* 1D Dirac strings, are decided by the charge-carrying DWs. The observed Dirac strings initially originated from the edge of the structure. In the presence of higher magnetic fields, the end points of the existing Dirac strings become the start points of new Dirac strings which further propagate into the lattice, *i.e.* no random flipping of the bars are observed in the middle of the structure. The results also show that opposite-charged monopoles hop in the opposite directions under the application of external field, similar to the motions of electrons and holes in semiconductors under the application of electric field. Our results will not only be useful in exploring the physics of monopoles but also for novel magnetic devices such as the data storage [5,32] and the logic devices [6] where the device efficiency is determined by the presence of the magnetic charges.

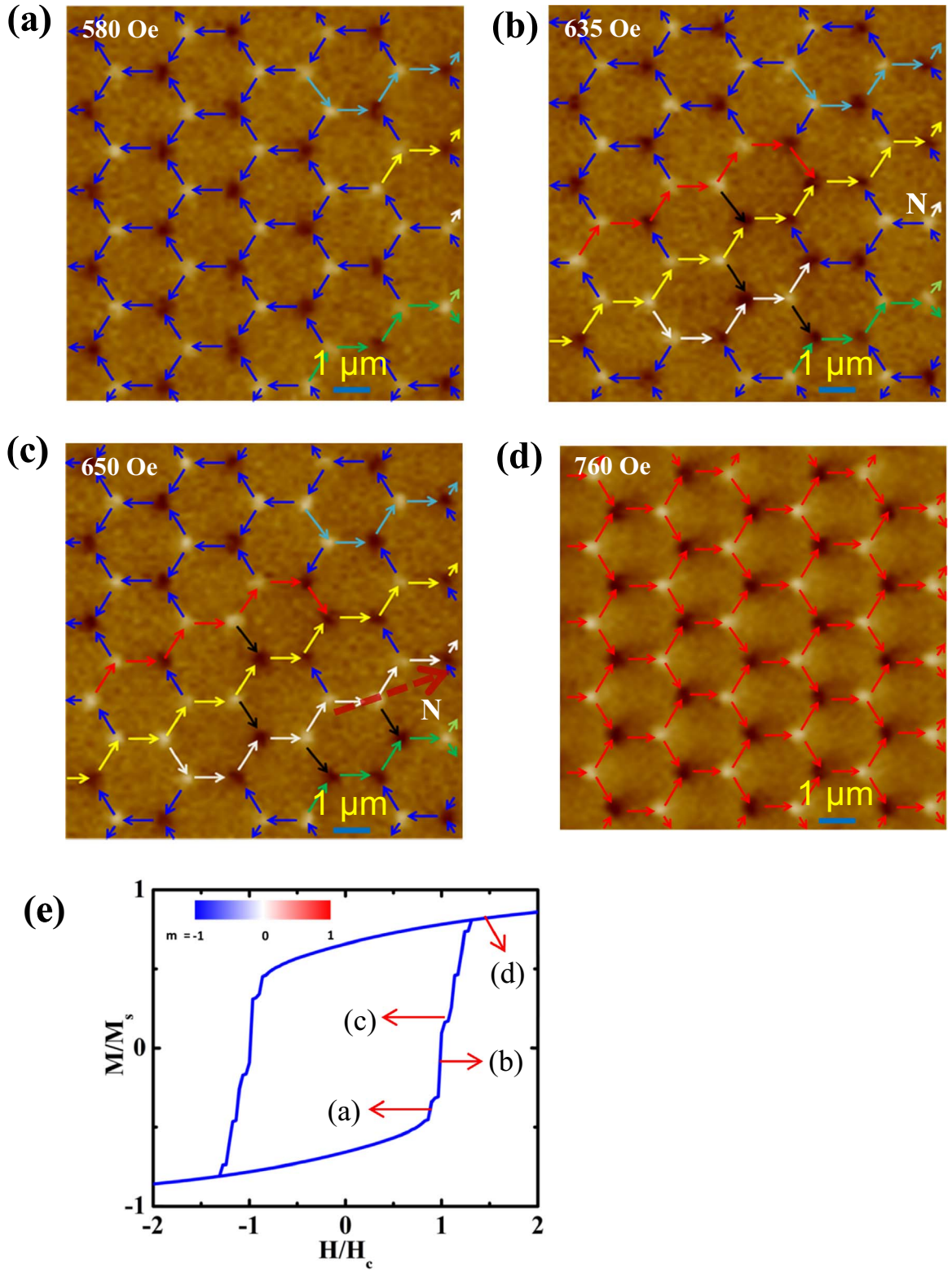

Fig. 4. Extension of the Dirac strings in the presence of external magnetic field. (a) New Dirac string (yellow) appears and starts to imprint its own path, while existing Dirac string is extended in length (aqua) at H_x=580 Oe. (b) Extensions of the Dirac strings in avalanche-like behavior at H_x=635 Oe. The strings are shown to be further extended in length through the formation and dissociation of monopoles. Additional Dirac strings (white and red) are also created within the structure (c) Extension of the white Dirac string at H_x=650 Oe (d) complete saturation of the artificial spin ice structure along the $+x$ direction at H_x=760 Oe. (e) The normalized hysteresis curve that is obtained from micromagnetic simulations, with the plateaus represent the trapped monopoles. 'H_c' is the coercivity of simulated spin ice network. Inset shows the magnetization scale. (For interpretation of the references to color in this figure legend, the reader is referred to the web version of this article.)

Acknowledgment

The work was supported by the NRF-CRP Program (Non-volatile Magnetic Logic and Memory Integrated Circuit Devices, NRF-CRP9-2011-01). Support from a MOE-AcRF Tier 2 Grant (MOE 2013-T2-2-017) is also acknowledged. The authors are also

thankful to Chandrasekhar Murapaka for his useful discussions and comments.

Appendix A. Supplementary material

Supplementary data associated with this article can be found in the online version at http://dx.doi.org/10.1016/j.jmmm.2016.07.005.

References

[1] P.A.M. Dirac, Proc. R. Soc. Lond. A 133 (1931) 60–72.
[2] D.J.P. Morris, D.A. Tennant, S.A. Grigera, B. Klemke, C. Castelnovo, R. Moessner, C. Czternasty, M. Meissner, K.C. Rule, J.-U. Hoffmann, K. Kiefer, S. Gerischer, D. Slobinsky, R.S. Perry, Science 326 (2009) 411–414.
[3] C. Castelnovo, R. Moessner, S.L. Sondhi, Nature 451 (2008) 42–45.
[4] L.D.C. Jaubert, P.C.W. Holdsworth, Nat. Phys. 5 (2009) 258–261.
[5] A. Pushp, T. Phung, C. Rettner, B.P. Hughes, S.-H. Yang, L. Thomas, S.S.P. Parkin, Nat. Phys. 9 (2013) 505.
[6] C. Murapaka, P. Sethi, S. Goolaup, W.S. Lew, Sci. Rep. 6 (2016) 20130.
[7] S.D. Bader, Rev. Mod. Phys. 78 (2006) 1–15.
[8] R.F. Wang, C. Nisoli, R.S. Freitas, J. Li, W. McConville, B.J. Cooley, M.S. Lund, N. Samarth, C. Leighton, V.H. Crespi, P. Schiffer, Nature 439 (2006) 303–306.
[9] X. Ke, J. Li, C. Nisoli, P.E. Lammert, W. McConville, R.F. Wang, V.H. Crespi, P. Schiffer, Phys. Rev. Lett. 101 (2008) 037205.
[10] S. Zhang, I. Gilbert, C. Nisoli, G.W. Chern, M.J. Erickson, L. O'Brien, C. Leighton, P.E. Lammert, V.H. Crespi, P. Schiffer, Nature 500 (2013) 553–557.
[11] Z. Budrikis, J.P. Morgan, J. Akerman, A. Stein, P. Politi, S. Lamgridge, C. H. Marrows, R.L. Stamps, Phys. Rev. Lett. 109 (2012) 037203.
[12] S.D. Pollard, V. Volkov, Y. Zhu, Phys. Rev. B 85 (2012) 180402(R).
[13] S.V. Isakov, R. Moessner, S.L. Sondhi, Phys. Rev. Lett. 95 (2005) 217201.
[14] A.P. Ramirez, A. Hayashi, R.J. Cava, R. Siddharthan, B.S. Shastry, Nature 399 (1999) 333–334.
[15] D. Bernal, R.H. Fowler, J. Chem. Phys. 1 (1933) 515–548.
[16] C. Castelnovo, R. Moessner, S.L. Sondhi, Annu. Rev. Condens. Matter Phys. 3 (2012) 35.
[17] S. Ladak, D.E. Read, G.K. Perkins, L.F. Cohen, W.R. Branford, Nat. Phys. 6 (2010) 359–363.
[18] E. Mengotti, L.J. Heyderman, A.F. Rodríguez, F. Nolting, R.V. Hügli, H.B. Braun, Nat. Phys. 7 (2011) 68–74.
[19] A.S. Wills, R. Ballou, C. Lacroix, Phys. Rev. B 66 (2002) 144407.
[20] K. Zeissler, S.K. Walton, S. Ladak, D.E. Read, T. Tyliszczak, L.F. Cohen, W. R. Branford, Sci. Rep. 3 (2013) 1252.
[21] Y. Shen, O. Petrova, P. Mellado, S. Daunheimer, J. Cumings, O. Tchernyshyov, New J. Phys. 14 (2012) 035022.
[22] S. Ladak, D. Read, T. Tyliszczak, W.R. Branford, L.F. Cohen, New J. Phys. 13 (2011) 023023.
[23] S.A. Daunheimer, O. Petrova, O. Tchernyshyov, J. Cumings, Phys. Rev. Lett. 107 (2011) 167201.
[24] A. Vansteenkiste, J. Leliaert, M. Dvornik, M. Helsen, F. Garcia-Sanchez, B. V. Waeyenberge, AIP Adv. 4 (2014) 107133.
[25] L.D. Buda, I.L. Prejbeanu, U. Ebels, K. Ounadjela, Comp. Mater. Sci. 24 (2002) 181–185.
[26] M. Kläui, C.A.F. Vaz, J.A.C. Bland, L.J. Heyderman, F. Nolting, A. Pavlovska, E. Bauer, S. Cherifi, S. Heun, A. Locatelli, Appl. Phys. Lett. 85 (2004) 5637–5639.
[27] D. Petit, A.V. Jausovec, H.T. Zeng, E. Lewis, L. O'Brien, D. Read, R.P. Cowburn, Phys. Rev. B 79 (2009) 214405.
[28] C. Nam, Y. Jang, K.-S. Lee, B.K. Cho, Nanotechnology 19 (2008) 015703.
[29] C. Phatak, A.K. Petford-Long, O. Heinonen, M. Tanase, M. De Graef, Phys. Rev. B 83 (2011) 174431.
[30] G. Mollar, R. Moessner, Phys. Rev. B 80 (2009) 140409(R).
[31] P. Mellado, O. Petrova, Y. Shen, O. Tchernyshyov, Phys. Rev. Lett. 105 (2010) 187206.
[32] S. Krishnia, I. Purnama, W.S. Lew, Appl. Phys. Lett. 105 (2014) 042404.